

Relic density calculations beyond tree-level, exact calculations versus effective couplings: the ZZ final state

F. Boudjema¹⁾, G. Drieu La Rochelle²⁾ and A. Mariano¹⁾

1) *LAPTh[†], Univ. de Savoie, CNRS, B.P110, F-74941 Annecy-le-Vieux, France*

2) *Univ. de Lyon, F-69622 Lyon, France; Univ. Lyon 1, Villeurbanne
CNRS/IN2P3, UMR5822, Institut de Physique Nucléaire de Lyon*

October 24, 2018

Abstract

The inferred value of the relic density from cosmological observations has reached a precision that is akin to that of the LEP precision measurements. This level of precision calls for the evaluation of the annihilation cross sections of dark matter that goes beyond tree-level calculations as currently implemented in all codes for the computation of the relic density. In supersymmetry radiative corrections are known to be large and thus must be implemented. Full one-loop radiative corrections for many annihilation processes have been performed. It is important to investigate whether the bulk of these corrections can be parameterised through an improved Born approximation that can be implemented as a selection of form factors to a tree-level code. This paper is a second in a series that addresses this issue. After having provided these form factors for the annihilation of the neutralinos into fermions, which cover the case of a bino-like LSP (Lightest Supersymmetric Particle), we turn our attention here to a higgsino-like dark matter candidate through its annihilation into ZZ. We also investigate the cases of a mixed LSP. In all cases we compare the performance of the form factor approach with the result of a full one-loop correction. We also study the issue of the renormalisation scheme dependence. An illustration of the phenomenon of non decoupling of the heavy sfermions that takes place for the annihilation of the lightest neutralino into ZZ is also presented.

LAPTh-019/14
LYCEN 2014-03

[†]UMR 5108 du CNRS, associée à l'Université de Savoie.

1 Introduction

There is circumstantial evidence [1–3] from different astrophysical and cosmological observations for the existence of Dark Matter (DM). In a particle physics context, the DM candidate can only be part of a theory of New Physics that has, alas, been elusive at the colliders so far [4, 5]. The next runs of the LHC will perhaps tell us whether the Higgs with a mass of 125 GeV is part of a richer underlying spectrum. Apart from its possible connection with the Higgs, in particular bringing in a solution to the naturalness problem, this New Physics may perhaps shed some light on the nature of Dark Matter. Although current LHC data set the scale of many New Physics scenarios in the TeV range [5], this inferred large scale refers in fact to the non observation of new coloured particles. On the one hand, the mass of the non coloured weakly interacting dark matter candidate is much less constrained from LHC analyses. On the other hand measurements of the relic density are now accurate at the per-cent level [2] and provide very strong constraints on the properties of DM. This supposes of course that we know the thermodynamics and cosmology of the universe, the standard approach for example incorporates thermal production but there are alternatives to the standard approach [6]. In any case, considering the per-cent precision on the relic density measurement, one needs to provide, from the particle physics side, dark matter annihilation cross sections at the per-cent level or better. State of the art codes [7–10] for the calculation of the relic density have been developed during the last decade. They are practically all based on tree-level cross sections and are therefore not precise enough. In some instances large corrections to the DM annihilation cross sections occur, for instance the classical Sommerfeld [11–15] effect or the electroweak Sudakov effect with the concomitant inclusion of final state radiation [16, 17]. These special effects are common to cases with TeV and above DM due to the presence of two disparate scales, the DM mass and a low mass mediator for which an example is the W gauge boson. In these regimes, the leading corrections that take into account these effects can be extracted. It remains that there are also important corrections in much more general situations irrespective of the mass of the DM. These corrections are far from being negligible, as shown in [16, 18–21].

For the last few years some of us have set up a programme [16, 18, 22] for the calculation of the full one-loop electroweak corrections for practically all annihilation channels of the Dark Matter candidate in the minimal supersymmetric model (MSSM). The first important ingredient of this programme requires a coherent and flexible renormalisation of all sectors of the MSSM, allowing for different renormalisation schemes. To be able to handle the large variety of possible annihilation and co-annihilation channels of the neutralino, a tool for the automated calculation of one-loop corrections in the MSSM was developed. This tool, SloopS [16, 19, 22, 23], based on [24–27], allows to perform full one-loop calculations [16, 18, 19, 23]. Ultimately the aim is to implement these corrections in a code such as micrOMEGAs [7] thus improving on the tree-level calculation of the annihilation cross sections. The difficulty is that one needs to correct some 3000 processes at one-loop in the case of the MSSM. Considering the large number of fields and parameters, the one-loop correction for each process requires computing a few hundred to a few thousands Feynman diagrams at one-loop. This is far more demanding than a computation at leading order. This is also totally intractable, for instance, in a scan over the parameter space. Yet, one can inquire whether the bulk of these corrections could be captured in a more compact form through effective form factor corrections to tree-level couplings. This would mean that these corrections are universal in the sense of being process independent and amount to an overall shift of the couplings of the different tree-level vertices. This improved Born approximation works quite well for LEP observables. Part of these corrections are for example due to the running of coupling constants but there might be other genuine corrections. If such an approximation works one could very easily recycle these improved Born couplings for any process which would very much improve a code such as micrOMEGAs. In Ref. [28] we explored whether this approach works in the case of the most simple of all annihilation channels, $\tilde{\chi}_1^0 \tilde{\chi}_1^0 \rightarrow f \bar{f}$, the annihilation of the neutralino into fermion pairs. In that case we introduced the effective vertices $\tilde{\chi}_1^0 f \bar{f}$ and $\tilde{\chi}_1^0 \tilde{\chi}_1^0 Z$ together with the improved vertex

$Zf\bar{f}$. Some of these effective vertices had also been discussed in [29, 30] outside the context of dark matter annihilation and later in [31]. Our first study revealed some very interesting results. In the case of a bino-like neutralino the percentage correction in the effective approach turned out to be a very good approximation falling short of about 2% compared to the full one-loop calculation. However as the bino component drops, the effective approach is a very rough approximation that worsens as the mass of the LSP increases, this is due to "non universal" rescattering effects (for example, box diagrams obtained from $\tilde{\chi}_1^0\tilde{\chi}_1^0 \rightarrow W^+W^-$ followed by $W^+W^- \rightarrow f\bar{f}$). However in these cases, the important point is that as the bino component drops the $\tilde{\chi}_1^0\tilde{\chi}_1^0 \rightarrow f\bar{f}$ is not an efficient annihilation channel, the largest channels being by far the annihilation processes of the neutralino into vector boson pairs. There is typically a factor of 10^4 between the two cross sections. In these scenarios, it is much more important to concentrate on annihilation to vector bosons, take the radiative corrections to $\tilde{\chi}_1^0\tilde{\chi}_1^0 \rightarrow W^+W^-, ZZ$ into account and implement $\tilde{\chi}_1^0\tilde{\chi}_1^0 \rightarrow f\bar{f}$ at tree-level, if at all. We must therefore pursue the implementation of an effective couplings approach to the annihilation into vector bosons. The aim of the present analysis is to concentrate first on $\tilde{\chi}_1^0\tilde{\chi}_1^0 \rightarrow ZZ$ before presenting our results for $\tilde{\chi}_1^0\tilde{\chi}_1^0 \rightarrow W^+W^-$, this will help us identify some new features without the need to worry, for example, about QED corrections and other complications that usually affect processes with charged particles. Another important point is that radiative corrections to neutralino annihilation are sensitive, even though only logarithmically, to the presence of heavy sfermions with masses far above those of the LSP. We discussed this point when we computed the radiative corrections to $\tilde{\chi}_1^0\tilde{\chi}_1^0 \rightarrow f\bar{f}$. So even if no coloured particles have been discovered at the LHC, meaning they may be in the TeV range, neutralino annihilation, if measured precisely, does probe their effect.

As we will see, the process $\tilde{\chi}_1^0\tilde{\chi}_1^0 \rightarrow ZZ$ is relevant when the $\tilde{\chi}_1^0$ has a fair amount of higgsino component. Therefore in our applications we consider a neutralino LSP with a mass in excess of 110 GeV to conform with the LEP limit on the chargino mass. For bino-like LSP this limit does not apply but, as we will see, for a bino-like LSP the process $\tilde{\chi}_1^0\tilde{\chi}_1^0 \rightarrow ZZ$ is not relevant. The LHC [32–35] may also provide some more stringent limits on the chargino/neutralino, however these are often model dependent. Even when LHC analyses are recast within a simplified model [36, 37], the limits are not necessarily applicable to our set-up, for example we work here with very heavy sleptons and squarks. Moreover the higgsino scenario is extremely challenging because of the small energy that is left for the visible tracks due to the small mass splitting within the higgsino system.

We will write t_β for $\tan\beta$. t_β , at tree-level, measures the ratio of the vacuum expectation values in the up to down sector. The crucial parameters for calculating $\tilde{\chi}_1^0\tilde{\chi}_1^0 \rightarrow ZZ$ are those of the neutralino/chargino sector, namely M_1, M_2 (respectively the $U(1)$ and $SU(2)$ soft gaugino masses at the electroweak scale) and μ , the higgsino mass parameter. Apart from these 3 parameters, and unless explicitly stated, we fix all other SUSY soft masses. The mass of the $SU(3)$ gaugino, M_3 , is set to 1 TeV. We take $t_\beta = 10$ and a common sfermion mass for both the left and right sfermions, $m_{\tilde{f}} = 800$ GeV. The tri-linear mixing parameter is set at $A_f = 2$ TeV for all sfermions. This high value is in fact of relevance for the third generation squarks, in particular the stop. The reason we take this value is to reproduce a Higgs mass in accord with that of the observed Higgs at the LHC. With our default parameters we obtain $M_h = 121.5$ GeV. This could be easily increased by taking heavier stops as will be done when we will study the “non decoupling” universal effects. Moreover, as we will see, Higgs exchange is subdominant in the scenarios we will cover and therefore, for the cross sections we study, sensitivity to the Higgs masses is negligible.

All cross sections are calculated for a centre of mass energy $s = 4M_{\tilde{\chi}_1^0}^2/(1 - v^2)$ with $v = 0.1$, which gives a relative scattering velocity $v_{\text{rel}} = 0.198 \sim 0.2$ as befits a relic density calculation. $M_{\tilde{\chi}_1^0}$ is the mass of the neutralino LSP.

2 $\tilde{\chi}_1^0 \tilde{\chi}_1^0 \rightarrow ZZ$ at tree-level, renormalisation and effective vertices

2.1 $\tilde{\chi}_1^0 \tilde{\chi}_1^0 \rightarrow ZZ$ at tree-level

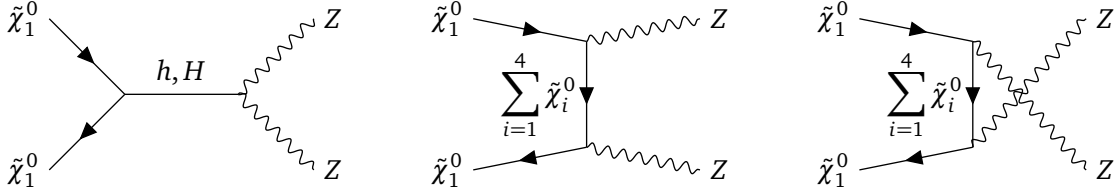


Figure 1: Diagrams contributing to the $\tilde{\chi}_1^0 \tilde{\chi}_1^0 \rightarrow ZZ$ annihilation at the tree level. h, H denote the lightest and heaviest CP-even Higgs, respectively.

The diagrams contributing to $\tilde{\chi}_1^0 \tilde{\chi}_1^0 \rightarrow ZZ$ at tree-level are shown in Fig. 1. In practically all cases, and certainly when $\tilde{\chi}_1^0 \tilde{\chi}_1^0 \rightarrow ZZ$ is a relevant annihilation channel, the largest contribution proceeds through the t -channel diagrams via the exchange of all neutralinos. The Higgs exchange contribution is then subdominant. The cross section is therefore largely driven by the strength of the $\tilde{\chi}_1^0 \tilde{\chi}_i^0 Z$ ($i = 1, \dots, 4$) vertex. First of all, at tree-level one has only the following structure

$$\mathcal{L}_{\tilde{\chi}_i^0 \tilde{\chi}_j^0 Z}^0 = \frac{g_Z}{4} \tilde{\chi}_i^0 \left\{ \left(N_{i3} N_{j3}^* - N_{i4} N_{j4}^* \right) \gamma_\mu P_R - \left(N_{i3}^* N_{j3} - N_{i4}^* N_{j4} \right) \gamma_\mu P_L \right\} \tilde{\chi}_j^0 Z^\mu, \quad g_Z = \frac{e}{c_W s_W}, \quad (1)$$

where $P_{R/L} = 1/2(1 \pm \gamma_5)$. N is the unitary complex matrix that defines the physical fields $\tilde{\chi}_i^0$, ($i = 1, \dots, 4$) in terms of the interaction eigenstates $(\psi^n)^t = (\tilde{B}^0, \tilde{W}^0, \tilde{H}_1^0, \tilde{H}_2^0)$ (respectively bino, wino and higgsinos)

$$\tilde{\chi}^0 = N \psi^n. \quad (2)$$

N diagonalises the mass mixing matrix of the neutralino sector Y , see [19] for details and conventions. As can be seen from Eq. 1, the strength of the $\tilde{\chi}_i^0 \tilde{\chi}_j^0 Z$ coupling is solely related to the higgsino component (note the presence of the matrix elements N_{i3} and N_{i4} in it). Therefore $\tilde{\chi}_1^0 \tilde{\chi}_1^0 \rightarrow ZZ$ is expected to play an important role, as an efficient annihilation channel, for a higgsino-like neutralino. From Eq. 2 we define the amount of bino, wino and higgsino of $\tilde{\chi}_1^0$ as follows

$$\tilde{\chi}_1^0 = N_{11} \tilde{B}^0 + N_{12} \tilde{W}^0 + N_{13} \tilde{H}_1^0 + N_{14} \tilde{H}_2^0, \quad (3)$$

which defines the bino, wino and higgsino fraction of $\tilde{\chi}_1^0$ as $f_B = |N_{11}|^2$, $f_W = |N_{12}|^2$, $f_H = |N_{13}|^2 + |N_{14}|^2$ respectively. The composition of the other neutralinos is defined in an analogous way.

We consider two cases of higgsino dominance. The higgsino-like scenario 1 is obtained by having $M_1 = 500$ GeV and $M_2 = 1$ TeV while μ is varied from 150 to 600 GeV. In this variation the LSP composition goes from higgsino-like to bino-like. As can be seen from Fig. 2 the change of the nature of the LSP is quite sudden and occurs at an LSP mass around 450 GeV.

In the second scenario, the higgsino-like scenario 2, we swap the values of M_1 and M_2 as compared to the first scenario, thus allowing for a transition from higgsino to wino, which occurs in this case around 400 GeV.

The last scenarios are bino-like and wino-like with $\mu = 1$ TeV while M_1 and M_2 are much smaller.

Fig. 2 confirms that $\tilde{\chi}_1^0 \tilde{\chi}_1^0 \rightarrow ZZ$ is indeed important for a higgsino-like LSP, being of order 10^2 pb for $f_H \sim 1$. In this case the $\tilde{\chi}_1^0 \tilde{\chi}_1^0 \rightarrow ZZ$ cross sections is of the same order as that of $\tilde{\chi}_1^0 \tilde{\chi}_1^0 \rightarrow W^+ W^-$ and is as much as 6 orders of magnitude larger than the cross section for the annihilation into fermion pairs. This overwhelming dominance is still present even when the higgsino content drops to 50%. At this level of higgsino content, $\tilde{\chi}_1^0 \tilde{\chi}_1^0 \rightarrow ZZ$ drops fairly quickly. In the first scenario, as some bino

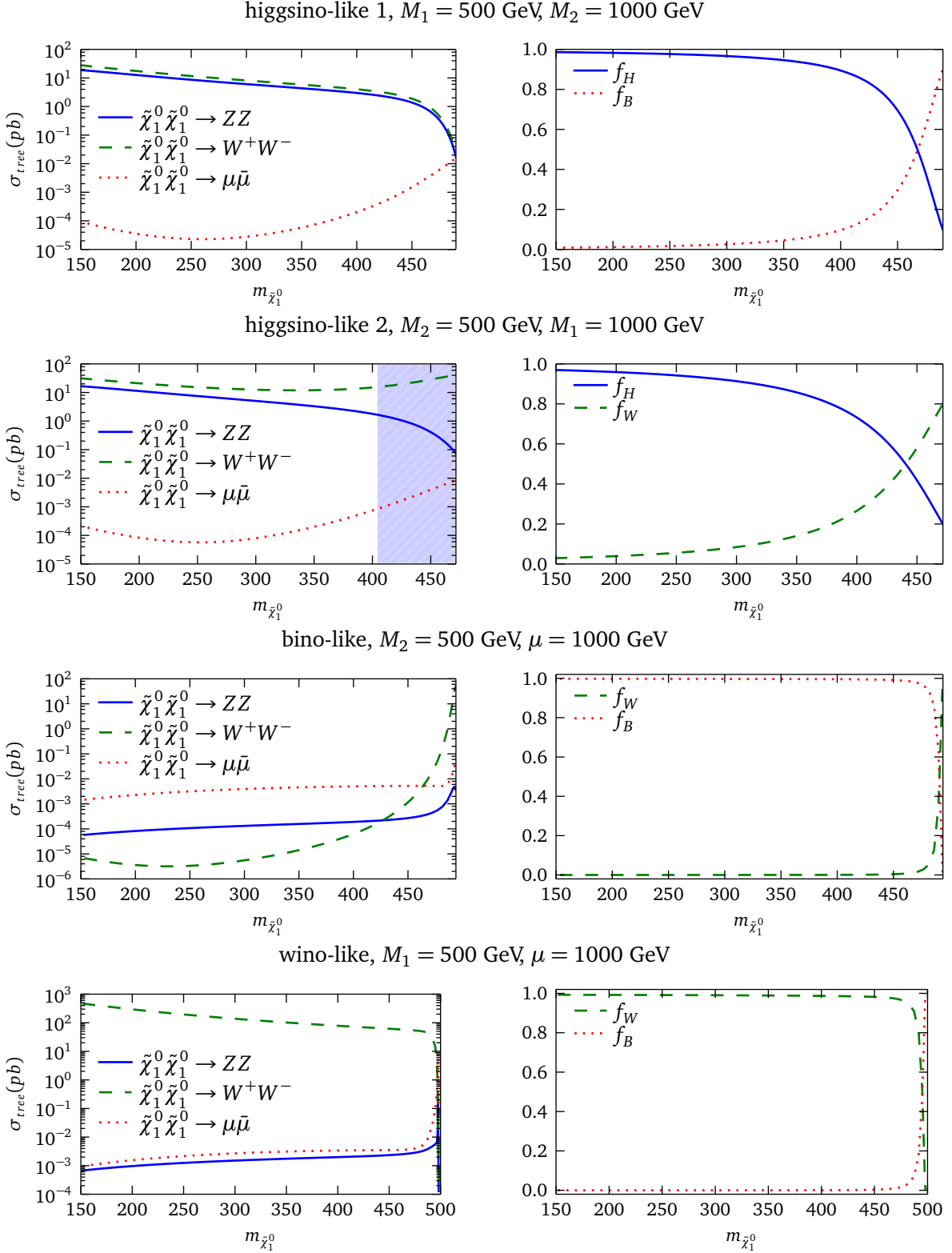


Figure 2: Tree-level annihilation cross sections (left panels) for a relative velocity of $v \simeq 0.2$ (see text) of the neutralino LSP for different masses and compositions (right panel). The characterisation higgsino-like, bino-like, wino-like stands for masses of the LSP below 400 GeV or so. The blue shaded area in the first figure of the second row corresponds to a contribution of $\tilde{\chi}_1^0 \tilde{\chi}_1^0 \rightarrow ZZ$ less than 10% of the total annihilation cross section (see text). For the bino and wino cases (3rd and 4th row) this is always the case. For the higgsino-like 1, first row, annihilation into ZZ is always larger than 10% in the mass range shown.

contamination feeds in for the highest LSP masses, $\tilde{\chi}_1^0 \tilde{\chi}_1^0 \rightarrow f \bar{f}$ starts picking up (due to the right slepton contribution) but without becoming competitive with $\tilde{\chi}_1^0 \tilde{\chi}_1^0 \rightarrow ZZ$ which remains of the same order as $\tilde{\chi}_1^0 \tilde{\chi}_1^0 \rightarrow W^+ W^-$. Note that in some scenarios and for some masses there might be other processes that enter the relic density calculation that are more effective, we can think of co-annihilation processes for example. We do not show them here. It is true that if these were non negligible they would reduce the weight of the $\tilde{\chi}_1^0 \tilde{\chi}_1^0 \rightarrow ZZ$. Each of the cross sections we display tracks a particular composition of the LSP: $\tilde{\chi}_1^0 \tilde{\chi}_1^0 \rightarrow f \bar{f}$ the bino, $\tilde{\chi}_1^0 \tilde{\chi}_1^0 \rightarrow ZZ$ the higgsino and $\tilde{\chi}_1^0 \tilde{\chi}_1^0 \rightarrow W^+ W^-$ the wino (even if the latter also contributes substantially in the higgsino case). Note that when we talk about $\tilde{\chi}_1^0 \tilde{\chi}_1^0 \rightarrow f \bar{f}$ we have essentially in mind the annihilation into charged leptons through right slepton exchange because they have the largest hypercharge.

The situation is somehow different in the second scenario: here, as expected, $\tilde{\chi}_1^0 \tilde{\chi}_1^0 \rightarrow W^+ W^-$ shoots up as the wino content increases while $\tilde{\chi}_1^0 \tilde{\chi}_1^0 \rightarrow ZZ$ drops continuously by 2 orders of magnitude within a range of 150 GeV in LSP mass and $\tilde{\chi}_1^0 \tilde{\chi}_1^0 \rightarrow f \bar{f}$ is always negligible. The wino nature starts affecting the cross-section at $f_H = 0.8$. This is easy to understand. In the pure wino limit $\tilde{\chi}_1^0 \tilde{\chi}_1^0 \rightarrow W^+ W^-$ is by far overwhelming, see for example the last set of figures in Fig. 2 for the wino-like scenario ($M_2 \ll (M_1, \mu)$). In the bino dominated region (scenario 3, $M_1 \ll (M_2, \mu)$), the largest cross section is $\tilde{\chi}_1^0 \tilde{\chi}_1^0 \rightarrow f \bar{f}$, $\tilde{\chi}_1^0 \tilde{\chi}_1^0 \rightarrow ZZ$ being a fraction of it, however as soon as there is even a small amount of wino component, $\tilde{\chi}_1^0 \tilde{\chi}_1^0 \rightarrow W^+ W^-$ takes off. In the wino dominated region (scenario 4, $M_2 \ll (M_1, \mu)$), $\tilde{\chi}_1^0 \tilde{\chi}_1^0 \rightarrow W^+ W^-$ is the only cross section of relevance being 6 orders of magnitude larger than $\tilde{\chi}_1^0 \tilde{\chi}_1^0 \rightarrow ZZ$. Here it is pointless to consider radiative corrections to $\tilde{\chi}_1^0 \tilde{\chi}_1^0 \rightarrow ZZ$ for the purpose of improving the calculation of the relic density.

As an aside, let us mention that the smallness of $\tilde{\chi}_1^0 \tilde{\chi}_1^0 \rightarrow f \bar{f}$ cross section is not only due to how small the bino content is in the higgsino region. Even when the bino content is large, the cross section is small compared to what we see for $\tilde{\chi}_1^0 \tilde{\chi}_1^0 \rightarrow ZZ$ in the higgsino region. Couplings left aside, compared to $\tilde{\chi}_1^0 \tilde{\chi}_1^0 \rightarrow ZZ$ and $\tilde{\chi}_1^0 \tilde{\chi}_1^0 \rightarrow W^+ W^-$, $\tilde{\chi}_1^0 \tilde{\chi}_1^0 \rightarrow f \bar{f}$ for massless fermions suffers from a chiral suppression that leads to a vanishing s -wave contribution. Moreover, t -channel processes are larger as the spin of the exchanged t -channel particle is large. The latter point gives an advantage to $\tilde{\chi}_1^0 \tilde{\chi}_1^0 \rightarrow ZZ$ mediated by a fermion rather than $\tilde{\chi}_1^0 \tilde{\chi}_1^0 \rightarrow f \bar{f}$ mediated by a sfermion, not to mention the fact that the exchanged sfermion is generally much heavier than the $\tilde{\chi}_1^0$ whereas for $\tilde{\chi}_1^0 \tilde{\chi}_1^0 \rightarrow ZZ$, $\tilde{\chi}_1^0 \tilde{\chi}_1^0 \rightarrow W^+ W^-$ in the higgsino region there is at least one of the neutralinos/charginos of very comparable mass to the LSP. Let us point also at another feature. In the higgsino region, say $\mu = 200$ GeV with $M_1 = M_2/2 = 500$ GeV, a 20% change in M_1 results in about 3% change in the cross section while the neutralino mass hardly changes. In the mixed region with $\mu = 450$ GeV, $M_1 = M_2/2 = 500$ GeV, a 20% change in M_1 results in practically 100% change in the cross section, while the mass of the LSP becomes as much as 50 GeV smaller. This means that the determination of M_1 (and μ) is crucial in this region. This will have a consequence on the scheme dependence in the neutralino sector. The t_β dependence is extremely mild either in the pure or mixed regions. From the observations we have just made on the tree-level cross sections, it is to be stressed that it is for higgsino-like LSP configurations that $\tilde{\chi}_1^0 \tilde{\chi}_1^0 \rightarrow ZZ$ is of relevance and it is for these configurations that the effective approach we are seeking should best approximate the full one-loop corrections.

Let us note that we have shown all cross sections as a function of the LSP mass, that is as a function of physical parameters that could be measured instead of the underlying parameters M_1, M_2, μ . The nature of the LSP is given by f_H, f_W , the higgsino and wino content. The latter could in principle be reconstructed from the decay of other neutralinos or the production of neutralinos at colliders. This is also important when we move to implementing the radiative corrections, where the physical masses, in particular that of the LSP, will be used as input parameters.

2.2 Beyond the tree-level, full vs the Form Factor effective approach

$\tilde{\chi}_1^0 \tilde{\chi}_1^0 \rightarrow ZZ$ at tree-level requires the computation of not more than 2 sets of diagrams (see Fig. 1). Moreover when $\tilde{\chi}_1^0 \tilde{\chi}_1^0 \rightarrow ZZ$ is an efficient annihilation channel, Higgs exchange is not relevant. A one-loop computation of the same process calls for hundreds of diagrams, a selection of these is shown in Fig. 3.

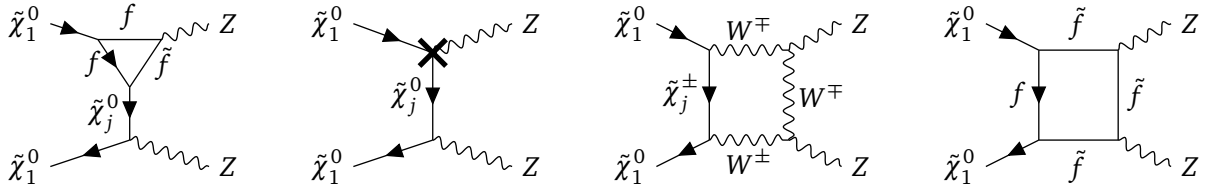


Figure 3: A selection of one-loop diagrams that contribute to $\tilde{\chi}_1^0 \tilde{\chi}_1^0 \rightarrow ZZ$. The first diagram is an example of a triangle of fermion/sfermion loops. The second is the implementation of a counterterm. The third is a box diagram of charginos and weak boson, note that it can be seen as $\tilde{\chi}_1^0 \tilde{\chi}_1^0 \rightarrow W^+ W^-$ followed by $W^+ W^- \rightarrow ZZ$. The last set consists of box diagrams of fermion/sfermions.

The first two diagrams of Fig. 3 can be considered as a universal correction to the $\tilde{\chi}_1^0 \tilde{\chi}_i^0 Z$ vertex through a fermion/sfermion loop to which counterterms are added. This is genuinely universal since these fermion/sfermion states do not relate to the external states. Needless to say that box diagrams are most time consuming in a numerical evaluation. Therefore if one can show that their contribution is small after all, the whole one-loop correction could be cast into a correction to vertices that were already needed for the tree-level calculation. If this is the case, one needs to replace the tree-level vertices, in particular the most important ones, namely $\tilde{\chi}_1^0 \tilde{\chi}_i^0 Z$, by an effective form factor vertex as shown in Fig. 4.

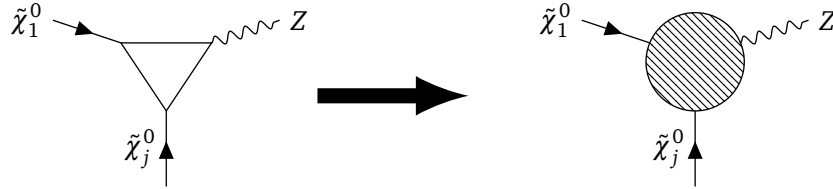


Figure 4: Example of the one-loop vertex diagrams that can be cast into an effective $\tilde{\chi}_1^0 \tilde{\chi}_j^0 Z$ vertex.

In this form factor approach, a single improved coupling could be used for any process, thus allowing an easy adaptation of tree-level codes. Nonetheless this does assume that the effective $\tilde{\chi}_i^0 \tilde{\chi}_i^0 Z$ vertex is just a rescaled version of the tree-level vertex defined in Eq. 1, with an overall replacement $\mathcal{L}_{\tilde{\chi}_i^0 \tilde{\chi}_j^0 Z}^0 \rightarrow \kappa_{ij} \mathcal{L}_{\tilde{\chi}_i^0 \tilde{\chi}_j^0 Z}^0$, κ_{ij} is the form-factor. This form factor can be obtained, as we show later, through modifications to the universal quantities g_Z and a new effective “mixing matrix” N that replace the tree-level values of Eq. 1 with $g_Z \rightarrow g_Z^{\text{eff}}$ and $N \rightarrow N^{\text{eff}}$. The approach does not allow for new Lorentz structures, otherwise the concept of an improved Born approximation would be meaningless.

At one-loop a full calculation of the one-particle irreducible (1PI) $\tilde{\chi}_i^0(k_i) \tilde{\chi}_j^0(k_j) \rightarrow Z_\mu$ vertex (triangle diagram), where the neutralino i carries momentum k_i , does in general yield new structures beside the ones present at tree-level. Therefore in general the induced one-loop corrected $\tilde{\chi}_i^0 \tilde{\chi}_j^0 Z$ would have the general form

$$\mathcal{L}_{\tilde{\chi}_i^0 \tilde{\chi}_j^0 Z}^0 \rightarrow \mathcal{L}_{\tilde{\chi}_i^0 \tilde{\chi}_j^0 Z}^0(g_Z \rightarrow g_Z^{\text{eff}}, N \rightarrow N^{\text{eff}}) + \tilde{\chi}_i^0 \left(K_1^{L,R} k_\mu^+ + K_2^{L,R} k_\mu^- \right) P_{R,L} \tilde{\chi}_j^0 Z^\mu, \quad k^\pm = k_i \pm k_j. \quad (4)$$

$K_{1,2}^{L,R}$ are new coupling strengths. For on-shell Z , like in $\tilde{\chi}_1^0 \tilde{\chi}_1^0 \rightarrow ZZ$, the structure k_μ^+ is of no relevance

(as a consequence of the on-shell spin-1 condition), while for $i \neq j$ a structure with k_μ^- could be present. One needs therefore to make sure that such new Lorentz structures give a negligible contribution. While these new Lorentz structures are necessarily ultraviolet finite without the need for renormalisation, corrections to a tree-level structure need, in general, renormalisation. An important ingredient is in fact given by the counterterms to the different parameters entering the process and the wave functions renormalisation, both effects calling for the evaluation of some 2-point functions. This is an example of the universal character of these contributions. In many instances these 2-point functions are sufficient for the evaluation of the universal form factor (as in $f\tilde{f}\tilde{\chi}_1^0$) without reference to the nature of the fermion/sfermion pair since the universal part only refers to the $\tilde{\chi}_1^0$. For $\tilde{\chi}_i^0\tilde{\chi}_j^0Z$, the 1PI vertex function is also needed in order to yield a finite result. We have already encountered this situation for the definition of the effective $\tilde{\chi}_1^0\tilde{\chi}_1^0Z$ coupling [28].

2.3 Renormalisation

In [16, 18, 19, 23] we gave a detailed presentation of our procedure for the renormalisation of all the sectors of the MSSM as implemented in our code for the automatic evaluation of one-loop corrections, SloopS [19, 22, 23]. We stick to an on-shell scheme generalising what is done for the Electroweak Standard Model [38]. All fermion and gauge boson masses are defined on-shell and the electric charge is defined in the Thomson limit. With our input parameters for the masses of the standard model fermions, the effective electric charge at the scale M_Z amounts to a correction of about 6.5%, therefore the running of α alone in $\tilde{\chi}_1^0\tilde{\chi}_1^0 \rightarrow ZZ$ would give a correction of about 13%. In the Higgs sector we take the mass of the neutral pseudo-scalar Higgs M_A as input while t_β is defined, as usual [23], from the decay process $A^0 \rightarrow \tau\tau$. Other schemes for t_β are possible [23]. For $\tilde{\chi}_1^0\tilde{\chi}_1^0 \rightarrow ZZ$, in particular in the higgsino case, the t_β scheme dependence is very mild and we will not discuss it here. In the case at hand what is most important in the renormalisation procedure are the key parameters that enter the neutralino sector, namely M_1, M_2, μ . In SloopS the default scheme is to choose two charginos masses $m_{\tilde{\chi}_1^\pm}$ and $m_{\tilde{\chi}_2^\pm}$ as input to define M_2 and μ and one neutralino mass to fix M_1 . In this scheme, the counterterms for the relevant parameters are [19]

$$\begin{aligned}\delta M_2 &= \frac{1}{M_2^2 - \mu^2} \left(\left(M_2 m_{\tilde{\chi}_1^+}^2 - \mu \det X \right) \frac{\delta m_{\tilde{\chi}_1^+}}{m_{\tilde{\chi}_1^+}} + \left(M_2 m_{\tilde{\chi}_2^+}^2 - \mu \det X \right) \frac{\delta m_{\tilde{\chi}_2^+}}{m_{\tilde{\chi}_2^+}} \right. \\ &\quad \left. - M_W^2 (M_2 + \mu s_{2\beta}) \frac{\delta M_W^2}{M_W^2} - \mu M_W^2 s_{2\beta} c_{2\beta} \frac{\delta t_\beta}{t_\beta} \right), \\ \delta \mu &= \frac{1}{\mu^2 - M_2^2} \left(\left(\mu m_{\tilde{\chi}_1^+}^2 - M_2 \det X \right) \frac{\delta m_{\tilde{\chi}_1^+}}{m_{\tilde{\chi}_1^+}} + \left(\mu m_{\tilde{\chi}_2^+}^2 - M_2 \det X \right) \frac{\delta m_{\tilde{\chi}_2^+}}{m_{\tilde{\chi}_2^+}} \right. \\ &\quad \left. - M_W^2 (\mu + M_2 s_{2\beta}) \frac{\delta M_W^2}{M_W^2} - M_2 M_W^2 s_{2\beta} c_{2\beta} \frac{\delta t_\beta}{t_\beta} \right),\end{aligned}\tag{5}$$

$$\begin{aligned}\delta M_1 &= \frac{1}{N_{1i}^2} \left(\delta m_{\tilde{\chi}_i^0} - N_{2i}^2 \delta M_2 + 2N_{3i}N_{4i} \delta \mu \right. \\ &\quad \left. - 2N_{1i}N_{3i} \delta Y_{13} - 2N_{2i}N_{3i} \delta Y_{23} - 2N_{1i}N_{4i} \delta Y_{14} - 2N_{2i}N_{4i} \delta Y_{24} \right),\end{aligned}\tag{6}$$

with $\det X = (M_2\mu - M_W^2 s_{2\beta})$. $\delta m_{\tilde{\chi}_i^0}$ is the counterterm of the i th neutralino defined entirely from its self-energy. In general, δO represents the counterterm for the parameter O . Note that both δM_2 and $\delta \mu$ could also be defined from the neutralino sector, by a simple generalization of Eq. 6. The definition of these counterterms reveals the presence of *denominators* such as $(M_2^2 - \mu^2)$ or N_{ij}^2 . One should therefore avoid such schemes in situations in which these denominators are very small. For example, if the LSP has a very small bino component one should in principle avoid taking its mass to define M_1 but rather choose a neutralino where this component is not negligible. This being said, considering that we are aiming

primarily at finding a good approximation for the higgsino case, the scheme dependence as concerns the best choice for defining M_1 is not an issue, as we shall see. On-shell renormalisation also requires that no-mixing between different physical fields remains after renormalisation of the parameters and that the physical fields are such that the residue at the pole of the propagators is one. This is achieved through wave function renormalisation for the neutralinos [19]

$$\tilde{\chi}_i^0 \rightarrow \tilde{\chi}_i^0 + \frac{1}{2} \sum_j \left(\delta Z_{ij} P_L + \delta Z_{ij}^* P_R \right) \tilde{\chi}_j^0. \quad (7)$$

These wave function renormalisation constants are particularly important for the definition of the effective couplings.

2.4 Implementation of the corrections for $\tilde{\chi}_i^0 \tilde{\chi}_j^0 Z$

From what we have just seen, the form factor includes the effects due to the renormalisation of the gauge couplings but also the effects due to the mixing between fields at one-loop (including renormalisation of the weak mixing angle and the mixing between the neutralinos). These are implemented through the self-energy 2-point functions of the various fields. To sum up, as advertised earlier, the effective form factor vertex is obtained by substituting $g_Z \rightarrow g_{\tilde{\chi}_i^0 \tilde{\chi}_j^0 Z}^{\text{eff}}$ and $N \rightarrow N + \Delta N$ with

$$\begin{aligned} \Delta N_{ij} &= \frac{1}{2} \sum_k N_{kj} \delta Z_{ki}, \quad (i, j, k) = 1 \dots 4, \\ g_{\tilde{\chi}_i^0 \tilde{\chi}_j^0 Z}^{\text{eff}} &= g_Z \left(1 + \Delta g_Z + \Delta g_{\tilde{\chi}_i^0 \tilde{\chi}_j^0 Z}^{\Delta} \right). \end{aligned} \quad (8)$$

δZ represents the various wave function renormalisations for the neutralino system (see Eq. 7) obtained solely through the set of two-point functions relative to the self-energies of the neutralinos. As such all arguments of these two-point functions are evaluated at the pole mass of the neutralinos. The full expressions are given in [19].

For the overall coupling g_Z we see that it involves two parts, Δg_Z and $\Delta g_{\tilde{\chi}_i^0 \tilde{\chi}_j^0 Z}^{\Delta}$. Similarly to the shift ΔN , Δg_Z is expressed solely in terms of the self-energies of the neutral gauge bosons. We have

$$\begin{aligned} \Delta g_Z \equiv \Delta g_Z(M_Z^2) &= \frac{1}{2} \left(\Pi'_{\gamma\gamma}(0) - 2 \frac{s_W}{c_W} \frac{\Pi_{\gamma Z}(0)}{M_Z^2} \right) + \frac{1}{2} \left(1 - \frac{c_W^2}{s_W^2} \right) \left(\frac{\Pi_{ZZ}(M_Z^2)}{M_Z^2} - \frac{\Pi_{WW}(M_W^2)}{M_W^2} \right) \\ &\quad - \frac{1}{2} \Pi'_{ZZ}(M_Z^2), \end{aligned} \quad (9)$$

where $\Pi_{VV'}$ with $V, V' = W, Z, \gamma$ denotes the self-energies of the gauge vector bosons. The combination of Δg_Z and ΔN , defined solely from two point-functions, does not lead to a finite result. In order to get a finite result we need to add a genuine three-point function contribution which we have labeled $\Delta g_{\tilde{\chi}_i^0 \tilde{\chi}_j^0 Z}^{\Delta}$. We have decided to extract this contribution from the amplitude of the one-loop transition $\tilde{\chi}_j^0 \rightarrow \tilde{\chi}_i^0 Z$ by identifying the corrections to the coefficients of the Lorentz structures that are already present at the tree-level.

It is important to stress that, for the form factor approximation, we only take into account leptons, quarks and their superpartners circulating into the loops. Loops involving gauge bosons and their superpartners have always been problematic and the problems are present even in the SM in the case of the $Z f \bar{f}$ process. In fact, in the approach we are using, it is difficult to extract a gauge independent value. This also leads to problems with unitarity. This would then require to include at least part of the box contribution but this contribution cannot be described in the simplified form factor approach.

The alert reader will have noticed that we have identified Δg_Z with $\Delta g_Z(M_Z^2)$. This is what would have been used for the decay $Z \rightarrow f\bar{f}$ and, since the Z is on-shell for $\tilde{\chi}_1^0 \tilde{\chi}_1^0 \rightarrow ZZ$, this is appropriate. Note that in [28] we had improved on this by using for $\tilde{\chi}_1^0 \tilde{\chi}_1^0 \rightarrow Z \rightarrow f\bar{f}$ a running Δg_Z evaluated at the invariant mass of the $f\bar{f}$ system. Here, in the same vein we have implemented the $g_{\tilde{\chi}_i^0 \tilde{\chi}_j^0 Z}^{\text{eff}}$ for two different scales that enter the contribution $\Delta g_{\tilde{\chi}_i^0 \tilde{\chi}_j^0 Z}^{\Delta}$. The scale relates to value of the invariant mass of the would be, in $\tilde{\chi}_1^0 \tilde{\chi}_1^0 \rightarrow ZZ$, intermediate neutralino. As we will see when performing the calculations in different scenarios, the difference in the corrected (effective) calculation is small between the two choices of scales that we are about to define.

- In the default implementation of the form factor approach, the $\tilde{\chi}_1^0 \tilde{\chi}_i^0 Z$ triangle vertex is evaluated on the mass shell for all three particles. Although $\tilde{\chi}_i^0 \rightarrow \tilde{\chi}_1^0 Z$ (that is needed for $\tilde{\chi}_1^0 \tilde{\chi}_1^0 \rightarrow ZZ$) is not always open kinematically, one may still, at the amplitude level, evaluate this transition with all external momenta on-shell. An advantage of this, is that once a model is defined and therefore all masses of neutralinos known, the form-factor is given once and for all for this model and could be applied to any kind of process where the vertex $\tilde{\chi}_1^0 \tilde{\chi}_i^0 Z$ is involved. In this implementation the effective coupling is simply denoted $g_{\tilde{\chi}_i^0 \tilde{\chi}_j^0 Z}^{\text{eff}}$ and $Q_{\tilde{\chi}_i^0}^2 = m_{\tilde{\chi}_i^0}^2$.
- One could think of slightly adapting the form factor to the kinematics of the $\tilde{\chi}_1^0 \tilde{\chi}_1^0 \rightarrow ZZ$ process by taking into consideration that for $\tilde{\chi}_1^0 \tilde{\chi}_1^0 \rightarrow ZZ$, the $\tilde{\chi}_i^0$ in the vertex $\tilde{\chi}_1^0 \rightarrow \tilde{\chi}_i^0 Z$ is off-shell with invariant mass $Q_{\tilde{\chi}_i^0}^2 \sim M_Z^2 - m_{\tilde{\chi}_1^0}^2$ (taking into account the small relative velocity of the LSP). In this case the effective coupling is denoted $g_{\tilde{\chi}_i^0 \tilde{\chi}_j^0 Z}^{\text{eff}}(Q_{\tilde{\chi}_i^0}^2)$.
- In order to quantitatively compare the effect of different implementation of the vertex, we have also implemented the new Lorentz structure (the k^- terms) together the effective coupling $g_{\tilde{\chi}_i^0 \tilde{\chi}_j^0 Z}^{\text{eff}}(Q_{\tilde{\chi}_i^0}^2)$. We will refer to this approximation as $\Delta_{f\tilde{f}}$. $\Delta_{f\tilde{f},no k^-}$ has no new Lorentz structure and corresponds therefore to $g_{\tilde{\chi}_i^0 \tilde{\chi}_j^0 Z}^{\text{eff}}(Q_{\tilde{\chi}_i^0}^2)$.

As we will see, the effect of the induced new Lorentz structures is totally negligible. This is a welcome feature since codes for the calculations of tree-level cross sections based on a tree-level Lagrangian can be used without implementing new structures and new rules, we will only need to pass the modified overall effective couplings. When we compare our results for the different approximations, FF stands for the form factor approach implemented directly in a tree-level calculator by exchanging the tree-level coupling by the improved one. Modifying the coupling in a cross section evaluator code from g_Z to $g_Z(1 + \delta g_Z)$ will inevitably incorporate contributions of order $(\delta g_Z)^2$. These should be small if the one-loop contribution is perturbative and, thus, makes sense. Nonetheless for corrections of order 10–20% of the tree-level calculation a form-factor implementation in a tree-level code that incorporates $\mathcal{O}((\delta g_Z)^2)$ can be off by 2–4%. We should allow for this when we compare the results with the full one-loop calculation which does not include higher order terms.

Contrary to the FF, in the implementation of $\Delta_{f\tilde{f}}$ and $\Delta_{f\tilde{f},no k^-}$ no quadratic terms of type $(\delta g_Z)^2$ are present. Therefore, beside the kinematics, with $\Delta_{f\tilde{f}}$ and $\Delta_{f\tilde{f},no k^-}$ we are following what is implemented within a full one-loop calculation, save for the fact that only leptons, quarks and their superpartners are kept in the loops.

Apart from the $\Delta_{f\tilde{f}}$ correction, the full one-loop calculation includes

- the set of all 2-point, 3-point and 4-point function contributions not involving leptons, quarks and their superpartners. This set will be referred to as $(\Delta + \square)_{no f\tilde{f}}$,
- box diagrams involving leptons, quarks and their superpartners as depicted in the last diagram of Fig. 3,

- one-loop corrections to the s -channel Higgs exchange contribution which is generally very small.

3 Analysis at one-loop

We now analyse the performance of the approximations compared to the results of the full one-loop corrections for all four types of scenarios that we described earlier when presenting the tree-level cross sections. The cross sections are evaluated as previously for $v \simeq 0.2$. When analyzing the one-loop results it is important to recall the tree-level behaviour and the LSP content as shown in Fig. 2 to which we urge the reader to refer to alongside the loop corrections we discuss below.

3.1 Higgsino-like cases

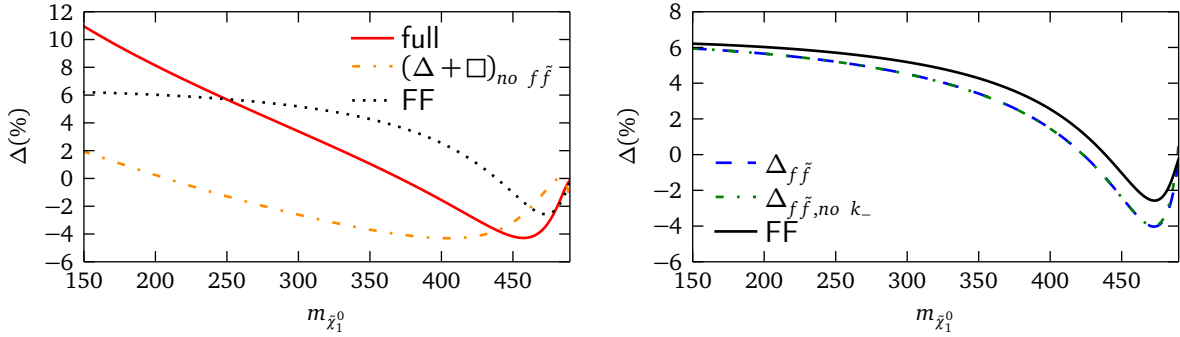


Figure 5: Radiative corrections as a function of the neutralino LSP mass for different approaches. Up to LSP masses around 400 GeV, the LSP is dominantly higgsino. Around 450 GeV the LSP turns into a bino-like LSP. The panel on the right compares the different implementations of the form factor approach (see the text for the meaning of the labeling).

As we can see from Fig. 5, in the case of a higgsino-like LSP, the full one-loop radiative corrections range from 11% (for the lightest masses) to -3% (for the heaviest LSP). The drop in the correction as the mass of the LSP increases is smooth. As the nature of the LSP turns into bino-like, we see a turn-over in the percentage correction. In the range of LSP mass between 450 and 500 GeV this correction increases slightly. This trend, with the turn over, is reproduced with the form factor (FF) approximation. In fact, the result that we obtain using the form factor is not far from the full correction even if it is more “flat” for small (less than 300 GeV) LSP masses. The largest discrepancy is observed for the lightest masses, 150 GeV, where we have a difference slightly above 4%. Otherwise the difference between the full result and the FF is well within 4%. A naive implementation through a running of α would accidentally be not a bad approximation for masses around 150 GeV, since this amounts to about a 13% correction. This implementation would however be off as the mass increases. Moreover, this will not show as much variation and structure as the effective FF and the full one-loop correction suggests. Note that the contribution of the $W/\tilde{\chi}^\pm$ boxes are small, they are not larger than 4%. The s -channel contribution (Higgs exchange) in this case is totally negligible. As for the different implementations of the effective approach, we see that the addition of a new Lorentz structure (k^- terms) is totally negligible. For most of the mass range, in particular for the whole range where the $\tilde{\chi}_1^0 \tilde{\chi}_1^0 \rightarrow ZZ$ cross section is large and the LSP is dominantly higgsino, the form factor approach and the $\Delta_{f \tilde{f}}$ agree very well. The largest difference shows up in the (uninteresting) bino-like region and amounts to no more than 1%.

We now turn to the second scenario of higgsino-like LSP’s and plot the results in Fig. 6. The difference with the previous case is that the LSP picks up more and more wino component as the mass the LSP increases. Compared to the previous case, the contamination due to the wino component starts

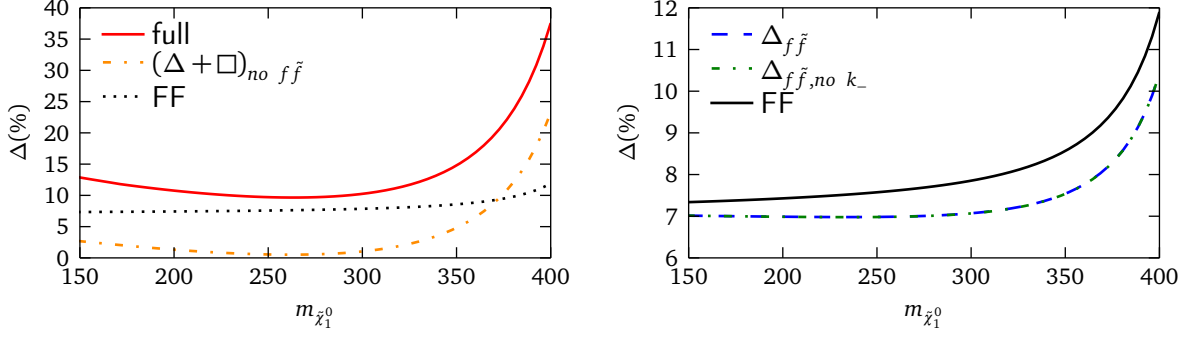


Figure 6: Higgsino LSP with some wino component, corresponding to the higgsino-like 2 scenario. The labeling is the same as in Fig. 5.

much earlier in the sense that the higgsino fraction drops more quickly. One must keep in mind that the tree-level cross section $\tilde{\chi}_1^0 \tilde{\chi}_1^0 \rightarrow ZZ$ is less than a tenth of $\tilde{\chi}_1^0 \tilde{\chi}_1^0 \rightarrow W^+W^-$ for LSP masses above 400 GeV. This is the reason we only consider the corrections to the $\tilde{\chi}_1^0 \tilde{\chi}_1^0 \rightarrow ZZ$ cross section for masses below 400 GeV. Up to neutralino masses of about 300 GeV the conclusions are the same as in the previous case. For example in the range $m_{\tilde{\chi}_1^0} = 200 - 300$ GeV, the difference between the full correction and the form factor approach is less than 4%. The difference increases very fast past 300 GeV. At 400 GeV, the FF correction is about 12% while the full correction is more than 35%. On the one hand, as the difference between the full one-loop and the FF starts growing, around 300 GeV, the ratio $\sigma_{\tilde{\chi}_1^0 \tilde{\chi}_1^0 \rightarrow ZZ} / \sigma_{\tilde{\chi}_1^0 \tilde{\chi}_1^0 \rightarrow W^+W^-}$ gets smaller, meaning that $\tilde{\chi}_1^0 \tilde{\chi}_1^0 \rightarrow ZZ$ is not so relevant for a relic density calculation. On the other hand we note that for the same reason the box contribution starts picking up and is certainly not negligible in this region. As the wino component increases, $\tilde{\chi}_1^0 \tilde{\chi}_1^0 \rightarrow W^+W^-$ becomes more and more important, consequently rescattering effects become important so that $\tilde{\chi}_1^0 \tilde{\chi}_1^0 \rightarrow ZZ$ is induced through $\tilde{\chi}_1^0 \tilde{\chi}_1^0 \rightarrow W^+W^-$ that rescatters to give $W^+W^- \rightarrow ZZ$. This is exactly the contribution of the wino/chargino boxes (see third diagram in Fig. 3). We will see this more explicitly when we will look at the loop corrections for a wino-like LSP annihilating to ZZ .

As for the previous case, any one-loop induced new Lorentz structure is totally negligible (see Fig. 6). Once more, the difference between the FF implementation (all particles on their mass-shell) and the vertex insertion with the invariant mass of the intermediate neutralino at the correct kinematical value for $\tilde{\chi}_1^0 \tilde{\chi}_1^0 \rightarrow ZZ$, is within 1%. In fact, this difference is much smaller than 1% for the large $\tilde{\chi}_1^0 \tilde{\chi}_1^0 \rightarrow ZZ$ cross sections corresponding to the largest higgsino content.

3.2 Bino-like LSP

Studying the radiative corrections to $\tilde{\chi}_1^0 \tilde{\chi}_1^0 \rightarrow ZZ$ in such scenarios is not particularly useful. In this scenario $f_H \sim 0$ and $\tilde{\chi}_1^0 \tilde{\chi}_1^0 \rightarrow ZZ$ accounts for much less than 10% of all annihilation channels. In fact, up to masses around 450 GeV $f_B \sim 1$ and $\tilde{\chi}_1^0 \tilde{\chi}_1^0 \rightarrow f\bar{f}$ dominates the annihilation cross section. Even before the wino component fully picks up, $\tilde{\chi}_1^0 \tilde{\chi}_1^0 \rightarrow W^+W^-$ increases (for masses past 450 GeV) and the contribution of $\tilde{\chi}_1^0 \tilde{\chi}_1^0 \rightarrow ZZ$ to the total annihilation rate is even smaller. Nonetheless it is perhaps worth to see where the corrections to $\tilde{\chi}_1^0 \tilde{\chi}_1^0 \rightarrow ZZ$ stem from. Considering the smallness of the tree-level $\tilde{\chi}_1^0 \tilde{\chi}_1^0 \rightarrow ZZ$, it is more appropriate to indicate how $\tilde{\chi}_1^0 \tilde{\chi}_1^0 \rightarrow ZZ$ is generated at one-loop. Indeed, for most part of the parameter space in this scenario the full correction is larger than 20%, it even reaches 100% for $m_{\tilde{\chi}_1^0} = 150$ GeV and even more for the highest masses when the LSP is wino-like. In the wino-like region (which we will study more specifically in the next section), rescattering effects through $\tilde{\chi}_1^0 \tilde{\chi}_1^0 \rightarrow W^+W^-$ become important, as we have seen in the last section. As Fig. 7 shows for $m_{\tilde{\chi}_1^0} > 450$ GeV, the full correction is driven by the $W/\tilde{\chi}^\pm$ loops, in particular by the box diagrams. For lower masses, when the LSP is bino, this rescattering is relatively small. Yet the FF fails

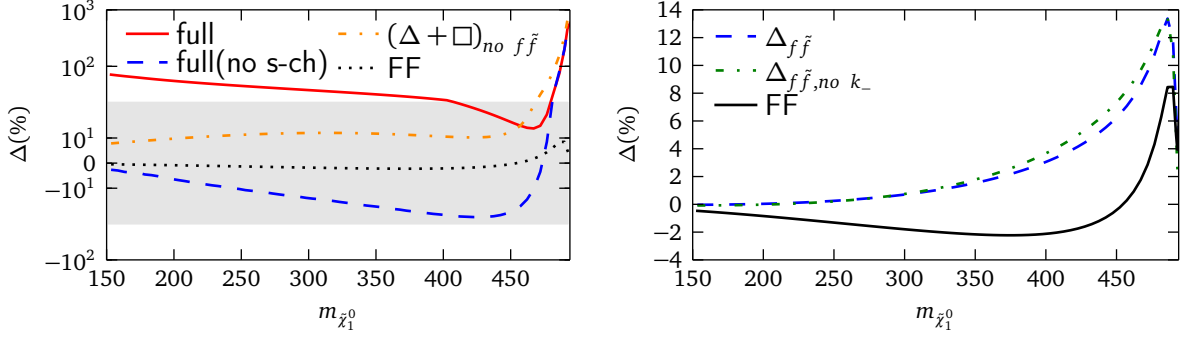


Figure 7: Results of a one-loop calculation in the case where the higgsino component is vanishing. For masses up to 450 GeV or so, the LSP is bino-like. Its nature changes suddenly to a wino-like LSP for masses greater than 450 GeV. Here we also show the results that one would obtain if the radiative corrections to the s -channel Higgs exchange are not taken into account, labeled as “full (no s -ch)”. The rest of the labeling is the same as in Fig. 5. The grey-shaded horizontal band corresponds to corrections within $\pm 20\%$, plotted using a linear scale.

completely in reproducing the full correction. What our study shows is that it is important to correct the s -channel Higgs exchange contribution in the bino case. Indeed leaving aside this correction gives a large discrepancy with the full correction. Note also that the FF implementation marginally reproduces the non s -channel Higgs exchange. One can therefore say that in this case the form factor result is not very reliable both in the wino and in the bino regions. Furthermore, our study reveals that there is an issue about which invariant mass one implements for the intermediate neutralino that is exchanged in the t/u channels. Although this is smaller than 2% for $m_{\tilde{\chi}_1^0} < 300$ GeV, the discrepancy increases to more than 4%. This of course is small detail and tiny discrepancy compared to the performance of the FF against the full one-loop correction. Once more, the effect of the new Lorentz structures in the vertex are totally negligible.

3.3 Wino-like LSP

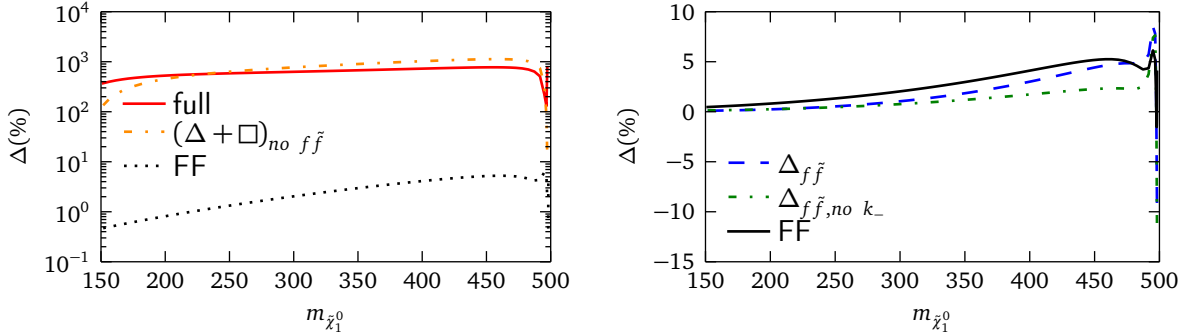


Figure 8: Same as in Fig. 5 for a wino-like LSP

In this scenario $\tilde{\chi}_1^0 \tilde{\chi}_1^0 \rightarrow ZZ$ is extremely small compared to the dominant $\tilde{\chi}_1^0 \tilde{\chi}_1^0 \rightarrow W^+ W^-$ cross section, the two cross sections are 6 orders of magnitude apart. Therefore for the relic density calculation there is no need to include $\tilde{\chi}_1^0 \tilde{\chi}_1^0 \rightarrow ZZ$. The reason we have looked at the one-loop corrections is just to make the previous observations about the importance of rescattering $\tilde{\chi}_1^0 \tilde{\chi}_1^0 \rightarrow W^+ W^-$ followed by $W^+ W^- \rightarrow ZZ$ more striking, as shown in Fig. 8. We can see that for practically all masses the full correction is driven by the $W/\tilde{\chi}^\pm$ loops and therefore the FF approach based on the leptons, quarks and superpartners loops is totally negligible. Of course in this case talking about radiative corrections

does not make much sense, considering that the effect of the loops amounts to “corrections” in excess of a few hundred per-cent of the tree level cross section. As we have argued previously, it is best to consider that for these cases $\tilde{\chi}_1^0 \tilde{\chi}_1^0 \rightarrow ZZ$ is induced through $\tilde{\chi}_1^0 \tilde{\chi}_1^0 \rightarrow W^+ W^-$. The important message in this wino scenario is that one must perform a one-loop correction on $\tilde{\chi}_1^0 \tilde{\chi}_1^0 \rightarrow W^+ W^-$ since this is by far the largest cross section. Co-annihilation processes should also be taken into account and we leave these studies for a forthcoming publication. Fig. 8 also shows that there is little difference between implementing the vertex correction through a full FF and a $\Delta_{f\tilde{f}}$ and that, once more, the effect of a new Lorentz structure although noticeable here, is below the 1%. These observations are of course an unimportant detail in view of the tiny effect of the entire effective vertex correction.

4 Renormalisation scheme dependence: the input neutralino masses

The summary so far is that $\tilde{\chi}_1^0 \tilde{\chi}_1^0 \rightarrow ZZ$ is an important annihilation channel as long as one is in the higgsino region and that, in this region, it is important to have a good prediction for this channel. In the higgsino-like scenarios we have seen that the FF approximation is quite a good one. One should then address the question of how much these conclusions, both for the full one-loop calculation and the FF approximation, depend on the renormalisation scheme. For the bino-like and wino-like scenarios this issue is of no importance since $\tilde{\chi}_1^0 \tilde{\chi}_1^0 \rightarrow ZZ$ is not an efficient annihilation channel.

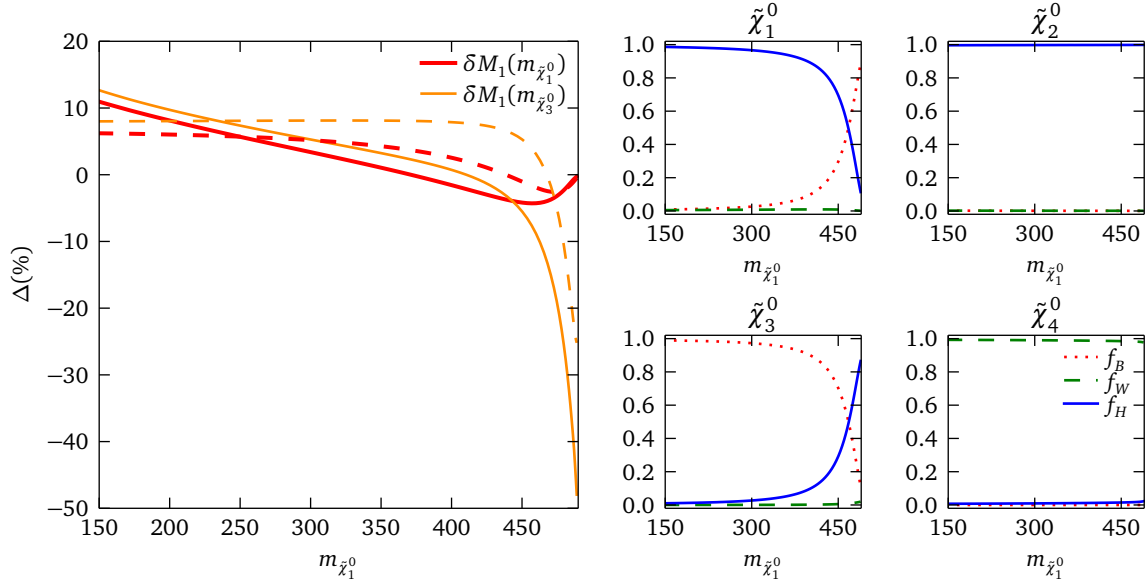


Figure 9: We compare the differences in the results for the percentage corrections between i) the default scheme where in the neutralino sector the LSP mass is taken as the input physical mass to reconstruct M_1 ($\delta M_1(m_{\tilde{\chi}_1^0})$) and ii) when the mass of the $\tilde{\chi}_3^0$ is taken as an input ($\delta M_1(m_{\tilde{\chi}_3^0})$). We do this for both the full set of the radiative corrections (solid line) and the form factor approach (dashed lines). The small panels on the right indicate the different compositions for each of the four neutralinos. Throughout the range, $\tilde{\chi}_4^0$ is, for all purposes, a wino while $\tilde{\chi}_2^0$ is higgsino. Up to $m_{\tilde{\chi}_1^0} = 450$ GeV, the LSP is higgsino-like and $\tilde{\chi}_3^0$ is bino-like, for masses beyond 450 GeV the roles of $\tilde{\chi}_1^0$ and $\tilde{\chi}_3^0$ are swapped.

First we briefly review the t_β scheme dependence. The default scheme is based on using $A^0 \rightarrow \tau \bar{\tau}$. Moving to a $\overline{\text{DR}}$ scheme [23] the changes are hardly noticeable. This is not surprising, recall our discussion on the t_β dependence of the tree-level results. We found that a change in t_β amounted to little effect on the cross section. In fact, the most crucial scheme dependence concerns the choice of the neutralino mass to define the counterterm for M_1 . In our default scheme, $m_{\tilde{\chi}_1^0}$ is used to reconstruct M_1 , the bino parameter. In the higgsino limit, $f_H \sim 1$, this choice does not, at first, seem to be a good

one since the bino component is very small. Indeed $N_{11} \sim 0$ in Eq. 6. However, a one-loop calculation of $\tilde{\chi}_1^0 \tilde{\chi}_1^0 \rightarrow ZZ$ is only crucial in the higgsino limit where what matters is a good reconstruction of μ , or rather the higgsino component. This is quite nicely extracted from the lightest chargino mass. Therefore in this limit since $\tilde{\chi}_1^0 \tilde{\chi}_1^0 \rightarrow ZZ$ depends very mildly on M_1 there should be no difference between the different schemes that are used in the neutralino sector to reconstruct δM_1 . Fig. 9 confirms these expectations in the scenario we call higgsino-like 1 where for masses up to $m_{\tilde{\chi}_1^0} = 450$ GeV the LSP is dominantly higgsino. We find that the δM_1 scheme dependence is totally negligible for the full one-loop results up to $m_{\tilde{\chi}_1^0} = 450$ GeV. If we compare a scheme where M_1 is extracted from the most bino-like neutralino, $\tilde{\chi}_3^0$, with the default scheme, we find a difference that is within 1% or so. The FF approximation follows the same trend although it looks like the agreement between the full one-loop and FF is slightly better when taking the LSP as input. Past a mass of 450 GeV, the transition towards a more bino-like takes place and the $\tilde{\chi}_1^0 \tilde{\chi}_1^0 \rightarrow ZZ$ cross section decreases. However once the transition occurs and the amount of bino in the LSP becomes relevant, the way in which we extract M_1 matters. We find that using $m_{\tilde{\chi}_3^0}$, instead of $m_{\tilde{\chi}_1^0}$ as input past 450 GeV leads to very large corrections and deviates significantly from the result of the default scheme. For $m_{\tilde{\chi}_1^0} \sim 480$ GeV the difference between using $m_{\tilde{\chi}_1^0}$ and $m_{\tilde{\chi}_3^0}$ for example is about 20%. This is much larger than the difference between the full one-loop and the effective coupling approach within the same scheme. The large M_1 scheme dependence in this bino configuration is directly related to the strong M_1 dependence of the tree-level cross section we pointed out in section 2.1. At the higgsino to bino transition point and above, it is perfectly sensible to keep using $m_{\tilde{\chi}_1^0}$, the now bino-like LSP mass, to define M_1 (N_{11} in Eq. 6 is no longer small). We therefore suggest to always use $m_{\tilde{\chi}_1^0}$ as the input parameter for $\tilde{\chi}_1^0 \tilde{\chi}_1^0 \rightarrow ZZ$ no matter what the composition of the LSP is. To summarize, whenever the higgsino component is large and $\tilde{\chi}_1^0 \tilde{\chi}_1^0 \rightarrow ZZ$ is of relevance, not only the FF is a good approximation but also, both for the full and the FF results, the scheme dependence is negligible.

5 Effects of very heavy sfermions and their non decoupling

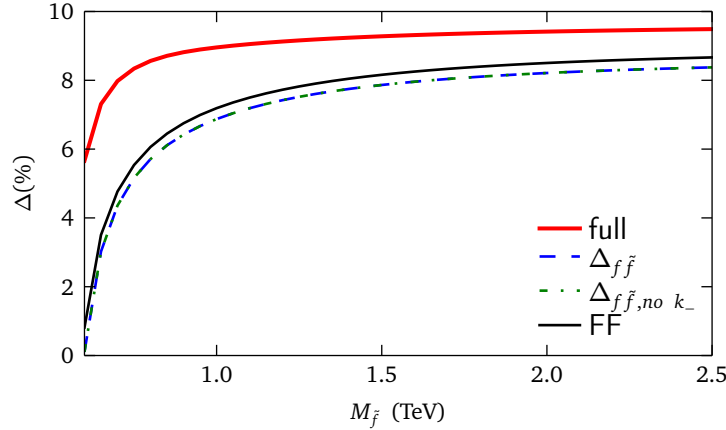


Figure 10: *Dependence of the full one-loop and effective radiative corrections on the common sfermion mass for a higgsino-like LSP. These points correspond to a neutralino of mass $m_{\tilde{\chi}_1^0} = 142.5$ GeV and components $(f_B, f_W, f_H) = (0.008, 0.005, 0.987)$.*

We argued in the introduction to this paper and we discussed more at length in [28] when analyzing $\tilde{\chi}_1^0 \tilde{\chi}_1^0 \rightarrow f \bar{f}$ that the annihilation cross section of interest for the relic density exhibits the effect of non decoupling of the very heavy sfermions which is a consequence of supersymmetry breaking and the fact that $m_{\tilde{\chi}_1^0} \ll m_{\tilde{f}}$. This non decoupling has been studied in a different context earlier [30, 39, 40]. Fig. 10

shows how the correction increases as the mass of the common sfermion mass increases from 500 GeV to 2.5 TeV. After a relatively rapid rise, the increase is mild, almost leveling off for multi-TeV masses of the sfermions. The variation in the fermion/sfermion masses is well reproduced by the effective couplings in the FF approach.

6 Fixing the mass of the LSP

Up to now we have presented our results as a function of the neutralino LSP mass, for masses up to 450 GeV. The LSP was for all purposes in a “pure” state (higgsino, bino or wino). Past 450 GeV its composition would, in most of the cases, change rather drastically. It is interesting to also investigate the corrections and the performance of the FF approximation by fixing the mass of the LSP while varying its composition. We do this for three values of the LSP mass, 110, 200, 400 GeV and generate points in the parameter space that correspond to neutralino LSP masses within 2 GeV around these values. Fig. 11

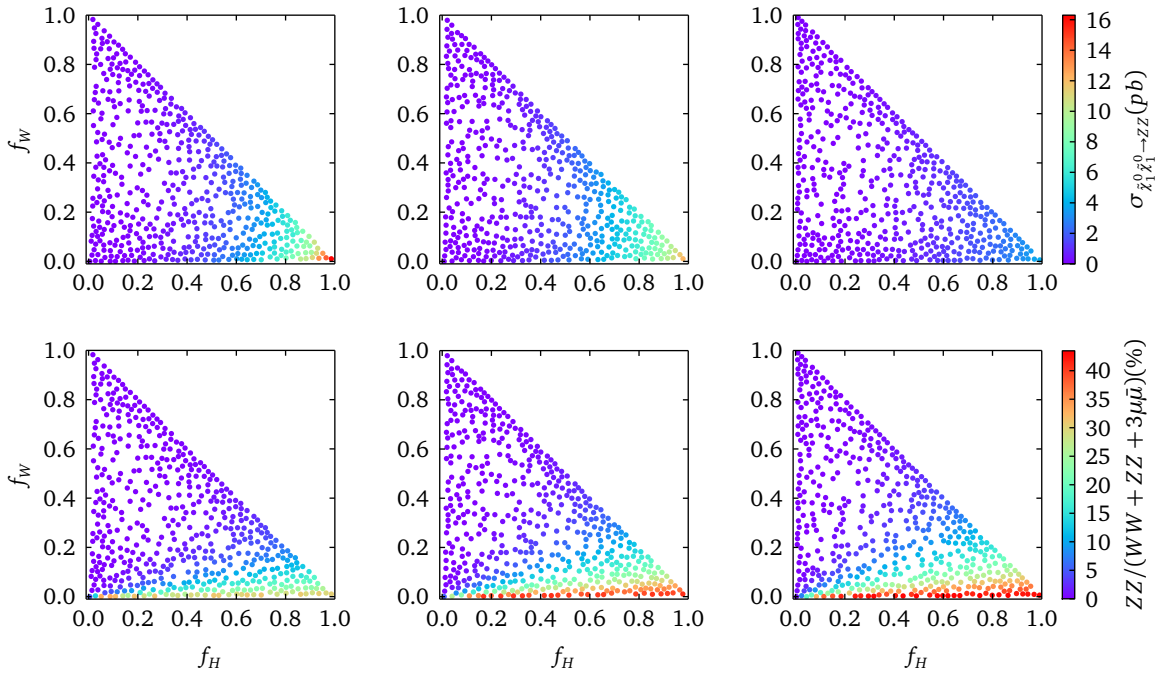


Figure 11: Annihilation cross section for the process $\tilde{\chi}_1^0 \tilde{\chi}_1^0 \rightarrow ZZ$ according to its wino and higgsino content for a neutralino of mass (from left to right panel) 110 , 200 and 400 (± 2) GeV and a relative scattering velocity $v \simeq 0.2$. We plot the tree-level cross section for $\tilde{\chi}_1^0 \tilde{\chi}_1^0 \rightarrow ZZ$ and its weight with respect to the $\tilde{\chi}_1^0 \tilde{\chi}_1^0 \rightarrow W^\pm W^\mp$ and $\tilde{\chi}_1^0 \tilde{\chi}_1^0 \rightarrow \mu \bar{\mu}$ cross sections.

does confirm that the largest cross sections do occur for the largest values of f_H . As the wino component grows, the cross section decreases for all three values of the LSP mass. In fact, as soon as $f_W > 0.2$, the relative weight of the $\tilde{\chi}_1^0 \tilde{\chi}_1^0 \rightarrow ZZ$ (normalized to $\tilde{\chi}_1^0 \tilde{\chi}_1^0 \rightarrow W^+ W^-$ and the annihilation into the three leptons, without including possible co-annihilation processes) drops below 10%. We consider that below this relative weight it is not important to get the full radiative correction since one should rather concentrate on getting as a precise a result as possible for the dominant annihilation process.

We have then assessed, whenever $\tilde{\chi}_1^0 \tilde{\chi}_1^0 \rightarrow ZZ$ is relevant, how the FF performs and how large the full radiative corrections can be. Fig. 12 shows that the FF approach performs best in the higgsino corner. In that corner the best results are obtained for $m_{\tilde{\chi}_1^0} = 200, 400$ GeV where the approximation is within 4% of the full result. The worst agreement is along a line with highest f_W and lowest f_H , as expected. However, with the restrictions we have imposed, namely to consider the radiative corrections

only for points that have $\tilde{\chi}_1^0 \tilde{\chi}_1^0 \rightarrow ZZ$ contribute more than 10%, there are only very few points where the disagreement is larger than 15%.

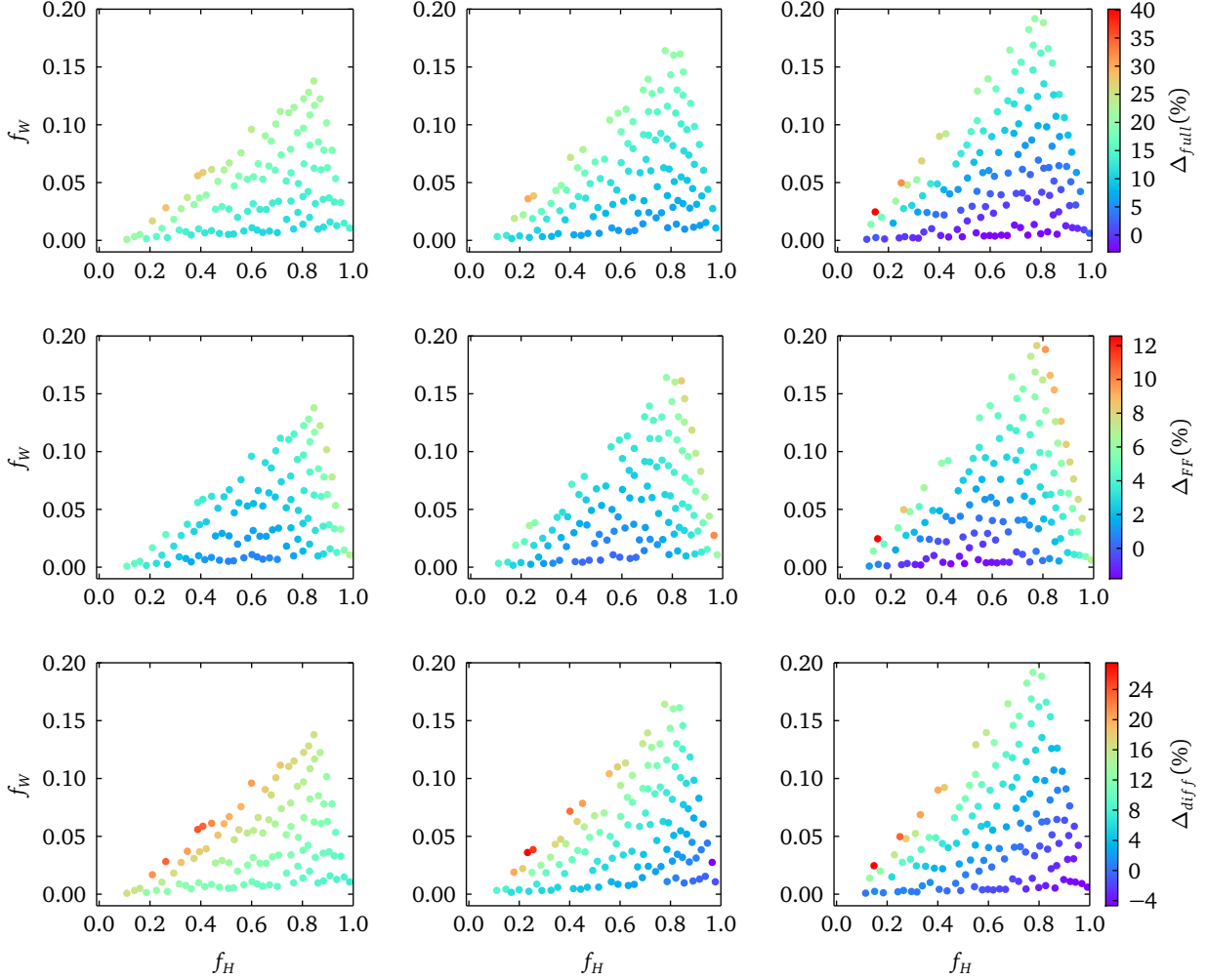


Figure 12: *Relative one-loop contributions to the tree level annihilation cross section for the process $\tilde{\chi}_1^0 \tilde{\chi}_1^0 \rightarrow ZZ$ corresponding to the tree-level cross sections given in Fig. 11. The panels are ordered in the same way as in Fig. 11. We plot the relative one-loop corrections obtained with the full one-loop calculation (first row), the form factor approach (second row) and the difference between the two (third row). We only consider those points for which the tree level cross section for the annihilation into ZZ is at least the 10% of the “total” cross section (see Fig. 11).*

7 Summary

Among all the constraints that are imposed on supersymmetry, for example through scans on the parameter space, the value of the relic density is the most stringent. The reason is most obvious. The current value on the relic density as extracted from a combination of cosmological measurements is at the percent level. Within the standard thermal cosmological model, this very accurate measurement translates into a very constraining bound on the cross sections involved in the annihilation of the LSP dark matter into Standard Model particles and hence on the underlying parameters of the supersymmetric model. Although this situation could be compared to the impact that the precision LEP measurements had on constraining many models of New Physics, the difference is that the experimental precision on the relic density is not matched by as precise theoretical calculations. The analyses still use predictions on

the relic density based on tree-level calculations of the annihilation cross sections and very often do not incorporate a theoretical uncertainty that accounts for the missing higher order calculations. Tools to perform one-loop calculations in supersymmetry do exist and their exploitation for the relic density computation have been achieved for many annihilation processes. It must however be recognized that such full one-loop calculations are lengthy and bulky: thousands of one-loop diagrams need to be evaluated, each one calling large libraries for one-loop integrals. Continuing our comparison with LEP, it is important to inquire whether a large part of the full one-loop corrections can be embedded in a minimal set of form factors that correct the tree-level couplings. This set of improved couplings can then be used for any process, not just the annihilation cross sections but also, for example, decays of some particles. If this programme can be realised it would be easy to exploit the same existing tree-level codes that are used for the relic density calculations. We initiated this program in a previous publication where we focused our attention on a bino-like scenario for the LSP where the most important channel is $\tilde{\chi}_1^0 \tilde{\chi}_1^0 \rightarrow f \bar{f}$. This has allowed to provide form factors for two important couplings of the neutralinos: $\tilde{\chi}_1^0 f \bar{f}$ and $\tilde{\chi}_1^0 \tilde{\chi}_1^0 Z$. In this paper we have considered $\tilde{\chi}_1^0 \tilde{\chi}_1^0 \rightarrow ZZ$ and in particular on extending the form factor library to $\tilde{\chi}_i^0 \tilde{\chi}_1^0 Z$, where $\tilde{\chi}_i^0$ can be any neutralino. The process $\tilde{\chi}_1^0 \tilde{\chi}_1^0 \rightarrow ZZ$ is also what characterizes a higgsino-like LSP. Of course, annihilation into vector bosons is more involved than annihilation into fermions and therefore it is very important to compare the results of the form factor approach to a full one-loop calculation. This is what we have performed in this paper. The results we find are very encouraging. We find that whenever annihilation to ZZ is relevant for the relic density, the form factor is a good approximation. In fact, for an almost pure higgsino the approach is very good. As the higgsino component degrades, the approximation becomes less and less reliable. This is even more so when the contamination is due to a wino component. However as the wino component gets large, $\tilde{\chi}_1^0 \tilde{\chi}_1^0 \rightarrow ZZ$ becomes inefficient as an annihilation channel. The cross section is tiny compared to the then dominant $\tilde{\chi}_1^0 \tilde{\chi}_1^0 \rightarrow W^+ W^-$ and therefore its weight in the relic density calculation becomes more and more marginal as the form factor approximation gets less and less precise. The dominance of $\tilde{\chi}_1^0 \tilde{\chi}_1^0 \rightarrow W^+ W^-$ is also the reason why the approximation fails. Indeed as we have shown, in these wino scenarios, one-loop box diagrams that are not accounted for by the form factor approach become important, if not dominant. This is due to what we called the rescattering effect. Indeed, in these cases $\tilde{\chi}_1^0 \tilde{\chi}_1^0 \rightarrow ZZ$ is generated through $\tilde{\chi}_1^0 \tilde{\chi}_1^0 \rightarrow W^+ W^-$ followed by $W^+ W^- \rightarrow ZZ$. The latter is a large cross section. The leading contribution from such effects could most probably be extracted in a compact form. We leave such improvement to a forthcoming analysis. Although the one-loop calculation of $\tilde{\chi}_1^0 \tilde{\chi}_1^0 \rightarrow ZZ$ is technically different from $\tilde{\chi}_1^0 \tilde{\chi}_1^0 \rightarrow f \bar{f}$, the conclusions about the performance of the form factors in the two cases are quite similar. Whenever the cross sections are efficient channels that contribute substantially to the relic density calculation, the form factor approach is a good approximation, in the sense that we reproduce the results within 4 – 5%. We have also checked that in these cases there are no large theory uncertainty due to the renormalisation scheme dependence. This good news encourages us to consider other scenarios and provide more form factors. The next important step, which we have already started, is a thorough investigation of the wino case through the important annihilation channel $\tilde{\chi}_1^0 \tilde{\chi}_1^0 \rightarrow W^+ W^-$. One should also add to the list some important co-annihilation channels, in particular those involving gauge bosons. The latter will be more relevant for higher LSP masses in both the wino and higgsino cases. In this paper we only considered LSP masses up to 500 GeV. The regime of (multi) TeV LSP requires a different approach that must address the large corrections of the Sudakov type and also in some cases the Sommerfeld effect as discussed in [13, 15–17].

Acknowledgments

We would like to thank Guillaume Chalons for many useful discussions. This research was supported in part by the French ANR project DMAstroLHC (ANR-12-BS05-0006), by the Labex ENIGMASS and by the European Commission through the HiggsTools Initial Training Network PITN-GA-2012-316704. AM

would like to thank the “Angelo della Riccia” Foundation for support.

References

- [1] N. Jarosik *et al.*, *Astrophys. J. Suppl.* **192** (2011) 14 [arXiv:1001.4744 [astro-ph.CO]].
- [2] Planck Collaboration, P. Ade *et al.*, (2013), [arXiv:1303.5076 [astro-ph.CO]].
- [3] B. A. Reid *et al.* [SDSS Collaboration], *Mon. Not. Roy. Astron. Soc.* **401** (2010) 2148 [arXiv:0907.1660 [astro-ph.CO]].
- [4] see for example, S. Caron for the ATLAS collaboration, arXiv:1106.1009 [hep-ex].
J. B. G. da Costa *et al.* [Atlas Collaboration], *Phys. Lett. B* **701** (2011) 186 [arXiv:1102.5290 [hep-ex]].
G. Aad *et al.* [ATLAS Collaboration], *Eur. Phys. J. C* **71** (2011) 1682 [arXiv:1103.6214 [hep-ex]].
S. Chatrchyan *et al.* [CMS Collaboration], [arXiv:1107.1279 [hep-ex]].
- [5] For an updated summary giving limits from the LHC on masses of particles from different models of New Physics, in particular from searches of coloured objects, see P. Bargassa, *Strong SUSY production searches at LHC*, Moriond 2013, Electroweak Session, <https://indico.in2p3.fr/conferenceOtherViews.py?view=standard&confId=9116>.
- [6] P. Salati, *Phys. Lett. B* **571** (2003) 121 [arXiv:astro-ph/0207396].
S. Profumo and P. Ullio, *JCAP* **0311** (2003) 006 [arXiv:hep-ph/0309220].
F. Rosati, *Phys. Lett. B* **570** (2003) 5 [arXiv:hep-ph/0302159].
C. Pallis, *JCAP* **0510** (2005) 015 [arXiv:hep-ph/0503080].
G. B. Gelmini and P. Gondolo, *Phys. Rev.* **D74** (2006) 023510 [arXiv:hep-ph/0602230].
D. J. H. Chung, L. L. Everett, K. Kong and K. T. Matchev, arXiv:0706.2375 [hep-ph].
M. Drees, H. Iminniyaz and M. Kakizaki, *Phys. Rev.* **D76** (2007) 103524, [arXiv:0704.1590 [hep-ph]].
A. Arbey and F. Mahmoudi, *JHEP* **1005** (2010) 051 [arXiv:0906.0368 [hep-ph]].
- [7] G. Bélanger, F. Boudjema, A. Pukhov, A. Semenov, *Comput. Phys. Commun.* **149** (2002) 103, hep-ph/0112278;
G. Bélanger, F. Boudjema, A. Pukhov, A. Semenov, *Comput. Phys. Commun.* **174** (2006) 577, hep-ph/0405253;
G. Bélanger, F. Boudjema, A. Pukhov, A. Semenov, *Comput. Phys. Commun.* **176** (2007) 367, hep-ph/0607059;
G. Bélanger, F. Boudjema, A. Pukhov and A. Semenov, *Comput. Phys. Commun.* **177** (2007) 894.
G. Bélanger, F. Boudjema, A. Pukhov and A. Semenov, *Comput. Phys. Commun.* **180** (2009) 747 [arXiv:0803.2360 [hep-ph]].
G. Bélanger, F. Boudjema, A. Pukhov, A. Semenov, *Comput. Phys. Commun.* **185** (2014) 960 [arXiv:1305.0237 [hep-ph]].
<http://lapth.cnrs.fr/micromegas>.
- [8] DarkSUSY: P. Gondolo *et al.*, *JCAP* **0407** (2004) 008, astro-ph/0406204;
<http://www.physto.se/~edsjo/darksusy/>.
- [9] SuperIso Relic: A. Arbey, F. Mahmoudi, A. Arbey and F. Mahmoudi, 1277 [arXiv:0906.0369 [hep-ph]].
Comput. Phys. Commun. **182**, 1582 (2011).
<http://superiso.in2p3.fr/relic/>.

- [10] F. Boudjema, J. Edsjo and P. Gondolo, in *Particle dark matter* 325-344, Oxford University Press (2010) G. Bertone, editor; Matter and at the Colliders,” [arXiv:1003.4748 [hep-ph]].
- [11] J. Hisano, S. Matsumoto, and M. M. Nojiri, Phys.Rev. **D67**, 075014 (2003), [arXiv:hep-ph/0212022].
- [12] R. Iengo, JHEP **0905**, 024 (2009), [arXiv:0902.0688 [hep-ph]].
- [13] N. Arkani-Hamed, D. P. Finkbeiner, T. R. Slatyer, and N. Weiner, Phys.Rev. **D79**, 015014 (2009), [arXiv:0810.0713 [hep-ph]].
- [14] A. Hryczuk and R. Iengo, JHEP **1201**, 163 (2012), [arXiv:1111.2916 [hep-ph]].
- [15] For a recent review see, A. Hryczuk, Phys. Lett. B **699** (2011) 271 [arXiv:1102.4295 [hep-ph]].
- [16] N. Baro, F. Boudjema, G. Chalons and S. Hao, Phys. Rev. D **81** (2010) 015005 [arXiv:0910.3293 [hep-ph]].
- [17] P. Ciafaloni *et al.*, JCAP **1310**, 031 (2013), [arXiv:1305.6391 [hep-ph]].
- [18] N. Baro, F. Boudjema, A. Semenov, Phys. Lett. **B660** (2008) 550, arXiv:0710.1821 [hep-ph].
- [19] N. Baro, F. Boudjema, Phys. Rev **D80** (2009) 076010, [arXiv:0906.1665 [hep-ph]].
- [20] A. Freitas, Phys. Lett. B **652** (2007) 280 [arXiv:0705.4027 [hep-ph]].
- [21] B. Herrmann and M. Klasen, in the Higgs Funnel,” Phys. Rev. D **76** (2007) 117704 [arXiv:0709.0043 [hep-ph]].
 B. Herrmann, M. Klasen and K. Kovarik, Annihilation into Massive Quarks with SUSY-QCD Corrections,” Phys. Rev. D **79** (2009) 061701 [arXiv:0901.0481 [hep-ph]].
 B. Herrmann, M. Klasen and K. Kovarik, beyond scalar or gaugino mass unification,” Phys. Rev. D **80** (2009) 085025 [arXiv:0907.0030 [hep-ph]].
- [22] F. Boudjema, A. Semenov, and D. Temes, Phys.Rev. **D72**, 055024 (2005), [arXiv:hep-ph/0507127].
- [23] N. Baro, F. Boudjema, A. Semenov, Phys. Rev. **D78** (2008) 115003, arXiv:0807.4668 [hep-ph].
- [24] A. Semenov. *LanHEP — a package for automatic generation of Feynman rules. User’s manual.*; hep-ph/9608488.
 A. Semenov, Nucl. Inst. Meth. and Inst. **A393** (1997) 293;
 A. Semenov, Comp. Phys. Commun. **115** (1998) 124;
 A. Semenov, hep-ph/0208011;
 A. Semenov, Comput. Phys. Commun. **180** (2009) 431, arXiv:0805.0555 [hep-ph].
- [25] J. Küblbeck, M. Böhm, A. Denner, Comp. Phys. Commun. **60** (1990) 165;
 H. Eck, J. Küblbeck, *Guide to FeynArts 1.0*, Würzburg, 1991;
 H. Eck, *Guide to FeynArts 2.0*, Würzburg, 1995;
 T. Hahn, Comp. Phys. Commun. **140** (2001) 418, hep-ph/0012260.
- [26] T. Hahn, M. Perez-Victoria, Comp. Phys. Commun. **118** (1999) 153, hep-ph/9807565;
 T. Hahn, hep-ph/0406288; hep-ph/0506201.
- [27] T. Hahn, LoopTools, <http://www.feynarts.de/looptools/>.
- [28] F. Boudjema, G. Drieu La Rochelle, and S. Kulkarni, Phys.Rev. **D84**, 116001 (2011), [arXiv:1108.4291 [hep-ph]].

- [29] J. Guasch, W. Hollik and J. Sola, JHEP **0210**, 040 (2002) [arXiv:hep-ph/0207364].
- [30] S. Kiyoura, M. M. Nojiri, D. M. Pierce and Y. Yamada, Phys. Rev. D **58**, 075002 (1998) [arXiv:hep-ph/9803210].
- [31] A. Chatterjee, M. Drees, and S. Kulkarni, Phys.Rev. **D86**, 105025 (2012), [arXiv:1209.2328 [hep-ph]].
- [32] CMS Collaboration, CMS-PAS-SUS-13-006 (2013).
- [33] ATLAS Collaboration, ATLAS-CONF-2013-049, ATLAS-COM-CONF-2013-050 (2013).
- [34] ATLAS Collaboration, ATLAS-CONF-2013-035, ATLAS-COM-CONF-2013-042 (2013).
- [35] CMS Collaboration, CMS-PAS-SUS-12-022 (2013).
- [36] S. Kraml *et al.*, (2013), [arXiv:1312.4175 [hep-ph]].
- [37] G. Aad *et al.* [ATLAS Collaboration], [arXiv:1403.5294 [hep-ex]], [arXiv:1402.7029 [hep-ex]].
- [38] G. Bélanger, F. Boudjema, J. Fujimoto, T. Ishikawa, T. Kaneko, K. Kato, Y. Shimizu, *Phys. Rep.* **430** (2006) 117, hep-ph/0308080.
- [39] H. C. Cheng, J. L. Feng and N. Polonsky, Phys. Rev. D **56** (1997) 6875, [arXiv:hep-ph/9706438];
idem Phys. Rev. D **57** (1998) 152, [arXiv:hep-ph/9706476].
- [40] E. Katz, L. Randall and S. f. Su, Nucl. Phys. B **536** (1998) 3 [arXiv:hep-ph/9801416].